Journal of Dental Research
2015, Vol. 94(4) 615–621

DOI: 10.1177/0022034515572189
jdr.sagepub.com

Enhanced Transport of Materials into Enamel Nanopores via Electrokinetic Flow

H.Y. Gan[1,2*], F.B. Sousa[3*], H.L. Carlo[4], P.P. Maciel[4], M.S. Macena[3], and J. Han[2]

Abstract

The ability to infiltrate various molecules and resins into dental enamel is highly desirable in dentistry, yet transporting materials into dental enamel is limited by the nanometric scale of their pores. Materials that cannot be infiltrated into enamel by diffusion/capillarity are often considered molecules with sizes above a critical threshold, which are often considered to be larger than the pores of enamel. We challenge this notion by reporting the use of electrokinetic flow to transport solutions with molecules with sizes above a critical threshold—namely, an aqueous solution with a high refractive index (Thoulet's solution) and a curable fluid resin infiltrant (without acid etching)—deep into the normal enamel layer. Volume infiltration by Thoulet's solution is increased by 5- to 6-fold, and resin infiltration depths as large as 600 to 2,000 μm were achieved, in contrast to ~10 μm resulting from diffusion/capillarity. Incubation with demineralization solution for 192 h resulted in significant demineralization at noninfiltrated histologic points but not at resin infiltrated. These results open new avenues for the transport of materials in dental enamel.

Keywords: dental enamel, histology, electroosmosis, nanofluidics, diffusion, dental bonding

Introduction

Water transport through nanometer scale channels has received considerable research interest (Duan and Majumdar 2010; Lee, Choi, et al. 2010; Wu et al. 2012), yet few biomedical applications of such concepts have been recognized so far. One of the recurring challenges in biomedicine is the effective delivery of drugs and biomolecules into various tissues. An extreme example of this can be found in the delivery of compounds through normal dental enamel with pore sizes in the range of 2 to 6 nm (Fig. 1).

Molecular and fluid transport through dental enamel is important in the context of several dental pathophysiologic processes, as well as various dental therapeutics and procedures. Transport of materials in wet dental enamel has been traditionally considered to be dependent on diffusion only (Poole et al. 1963; Shellis and Dibdin 2000). For a given flow velocity, the required pressure gradient is inversely proportional to the fourth power of the radius of the tube (Schoch et al. 2008). With nanometric pore sizes, enamel would require extremely high pressures for hydrostatic flow to occur, making its application for enhanced transport impossible. This is why the transport of ions or substances into enamel nanochannels in the majority of the literature was considered to rely mainly on slow diffusion. Empirically, molecules that are not penetrated by diffusion/capillarity are often regarded as molecules with sizes above a critical threshold (MACTs) and thought to be not able to infiltrate enamel pores (Shellis and Dibdin 2000).

As an informative reference for the currently known limits of transport of materials in enamel by diffusion, aqueous solutions with a mixture of mercury iodide and potassium iodide (known as Thoulet's solutions, whose complex ions HgI^{+}, HgI_2^{0}, HgI_3^{-}, and HgI_4^{2-} have radii of ~ 0.5 nm) and with high refractive index (RI ≥ 1.5) have been reported either not to infiltrate into enamel pores (Angmar et al. 1963; Theuns et al. 1993) or to infiltrate partially (up to 10%; Gwinnett 1966; Houwink 1969). Furthermore, resin adhesives (mainly composed of acrylate/methacrylate resin monomers) were thought to require an enlargement of enamel pores by acid etching to allow their infiltration (Hannig et al. 2002). Little progress has been made to enhance material transport through enamel nanopores. Recent reports demonstrated accelerated uptake of fluoride in enamel by using the principles of dielectrophoresis (Ivanoff et al. 2011; Ivanoff et al. 2012), where a modest

[1]Singapore Institute of Technology, Singapore Institute of Manufacturing Technology, Singapore
[2]Department of Electrical Engineering and Computer Science / Department of Biological Engineering, Massachusetts Institute of Technology, Cambridge, MA, USA
[3]Department of Morphology, Health Sciences Center, Federal University of Paraiba, Joao Pessoa, Cidade Universitaria, Paraíba, Brazil
[4]Department of Restorative Dentistry, Health Sciences Center, Federal University of Paraiba, Joao Pessoa, Cidade Universitaria, Paraíba, Brazil
*Authors contributing equally to this article.

A supplemental appendix to this article is published electronically only at http://jdr.sagepub.com/supplemental.

Corresponding Author:
J. Han, Rm 36-841, Massachusetts Institute of Technology, 77 Massachusetts Avenue, Cambridge, MA 02139, USA.
Email: jyhan@mit.edu

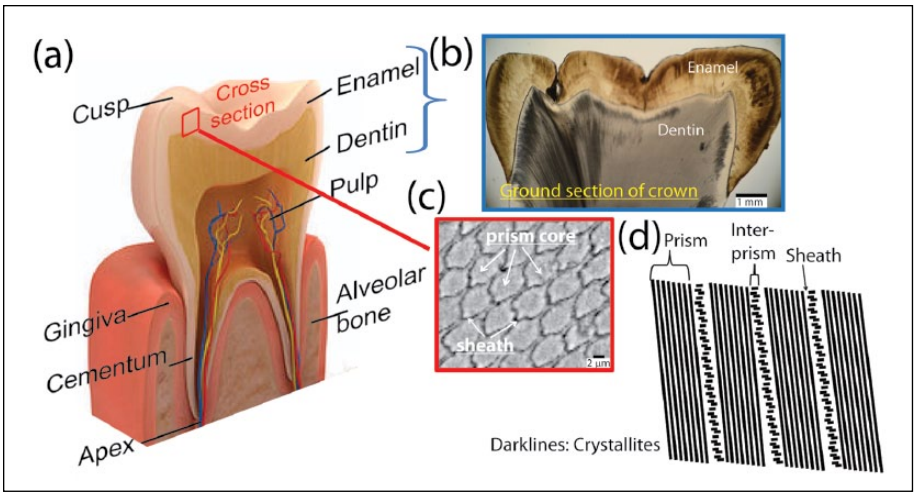

Figure 1. Diagram of enamel and its pores. (**a**) Anatomy of a mature human tooth. (**b**) Light microscopy image of ground section of tooth crown showing enamel, dentin, enamel-dentin junction, and an outline of enamel prisms. (**c**) Cross section of enamel prisms showing prism core and sheaths and (**d**) line drawing of hydroxyapatite crystallites as oriented in prismatic and interprismatic enamel (with smaller pores, 2 to 3 nm) separated by prism sheaths (with larger pores, 4 to 6 nm) (Zahradnik and Moreno 1975; Shellis and Dibdin 2000). Tooth anatomy figure: Science Picture Company.

infiltration (~50 µm) was reported but the transport of MACTs was not shown. Here, we explore the electric field–driven flows known as electrokinetic (EK) flow. Different from dielectrophoresis, which exerts a force on a dielectric particle when it is subjected to a nonuniform electric field, EK flow is the motion of liquid induced by an applied potential across a porous material, and this has been widely utilized in micro-/nanofluidic systems for decades (Sparreboom et al. 2012).

The aim of this study was to test the hypothesis that EK flow is able to significantly enhance transport of materials, even MACTs, into wet normal enamel pores without previous acid etching. To our knowledge, this is the first attempt to enhance material transport through the dental enamel layer using EK flow.

Materials and Methods

Microfluidic Chip Fabrication

The microfluidic chips consisted of 4 reservoirs, a sample seat, a thin ground section of enamel (thickness: 100 µm), and a sealing layer (Fig. 2a). A microfluidic sample seat and its sealing layer were fabricated in polydimethylsiloxane (PDMS) polymer (Sylgard 184, Dow Corning, Midland, MI, USA) using standard soft-lithographic microfabrication techniques. First, the microchannel layout was fabricated on a silicon wafer by using a photolithographic method with SU8-negative photoresists (SU-8 2035, MicroChem Inc., Newton, MA, USA). The patterned silicon wafer acted as a master mold for repeated device casting. It was then silanized with trichloro-(1H,1H,2H,2H-perfluorooctyl)-silane (Sigma-Aldrich, St. Louis, MO, USA) for 1 h before being used to aid the release of cast PDMS microchannels. Reservoir access holes (diameter of 1.5 mm) were also punched (Biopsy Inc.) on the sample seat layer. Prior to the insertion of an enamel section sample into the seat, a small volume of liquid PDMS was carefully applied to the seat chamber and 1 surface of enamel (the side of which was to be in contact with the sealing layer). Finally, the half-assembled device and the PDMS sealing layer underwent plasma treatment (Expanded Plasma Cleaner, Harrick Plasma, Ithaca, NY, USA) together for 2 min before being pressure bonded (~110 g dead weight) with heat (~75 °C) for 6 h. Four reservoirs were prepared from commercial pipette tips (Round tip, VWR, Radnor, PA, USA), with 2 working reservoirs with ~60 µL of volume placed at both ends of the enamel sample and the other 2 supplementary reservoirs with ~100 µL being connected to the working reservoirs via internal connecting channels (500-µm width × 100-µm depth) on each side (Fig. 2b). The purpose of supplementary reservoirs was to minimize the water level drop in the working reservoir during the lengthy infiltration operation.

EK Infiltration Test Setup

EK infiltration experiments with microfluidic chips were carried out with a Keithley source meter 2400 (Keithley Inc., Cleveland, OH, USA) connected to 2 Ag/AgCl electrodes serving as anode and cathode, respectively. The electrodes were inserted into the respective reservoirs of the chips close to both ends of an enamel ground section. Keithley LabTracer 2.0 control software was used with the source meter to control the required applied voltage for EK pumping and to record the corresponding system current during the course of experiment.

Enamel Sample Preparation

Unerupted third human molars were collected from volunteers (18 to 30 y old) who signed an informed consent form. The study was approved by the ethical committee on research in humans at the Hospital Lauro Wanderley of the Federal University of Paraíba (Brazil). Two types of samples of mature normal enamel were used: undemineralized ground sections with a thickness of ~100 µm (for experiments with microfluidic chips), prepared as described elsewhere (De Medeiros et al. 2013), and a whole tooth crown (for the resin infiltration only).

For microfluidic chip experiments, the enamel ground sections (with a dimension of ~1.5 mm × 500 µm × 100 µm, see Fig. 2c, d) were prepared by removing dentin from the tooth

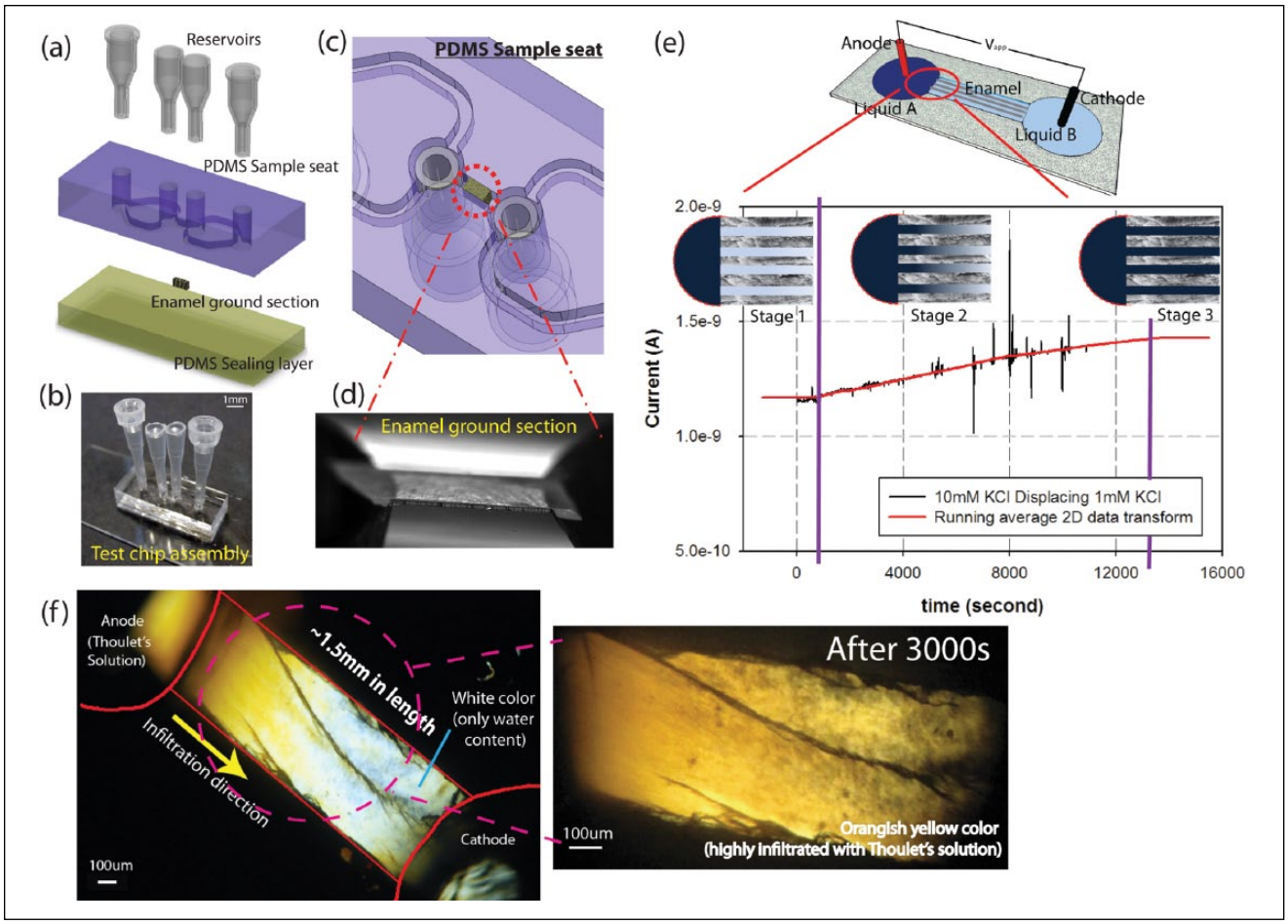

Figure 2. Experiments with enamel ground sections. (**a**, **c**) Device schematic, snapshots of (**b**) final assembly of microfluidic-aided test vehicle and (**d**) a typical processed enamel ground specimen with a dimension of 1.5 mm × 500 µm × 100 µm. (**e**) Typical displacement flow of 1mM (liquid A, anodic reservoir) and 10mM potassium chloride (KCl; liquid B, cathodic reservoir) solutions of a enamel sample at V_{app} = 1 V. Progression of electrokinetic-driven infiltration of liquid A (which replaces liquid B in enamel nanopore, therefore increasing overall conductivity and resulting in current increase) at different stages is depicted in small inserts, where colored lines (nongray areas) represent the enamel pores. (**f**) Snapshots of birefringence imaging for electrokinetic injection of high–refractive index (1.56) Thoulet's solution at operation after 2,000 s. Thoulet's solution was found at the enamel (anodic infiltration entrance) with color changes from white (with only water content) to yellowish (replaced by Thoulet's solution). Small insert shows the image at operation after 3,000 s; color was changed to orangish yellow, indicating high replacement of Thoulet's solution. In fact, this represents the complete infiltration of Thoulet's solution as far as 1.5 mm into the enamel ground section. The black lines (f) indicate lamellas, which consist of linear defect filled with organic matters and can be found in normal enamel (Nanci 2012). PDMS, polydimethylsiloxane.

ground sections using a stainless-steel blade under the stereomicroscope. Dentin removal was confirmed by the absence of fluorescence under fluorescence microscopy.

Microfluidic Chip Experiments with Enamel Ground Sections

The enhanced mass transport and effectiveness of infiltration by EK pumping were evaluated by the current monitoring method (for potassium chloride [KCl] infiltration) and optical birefringence measurement (for infiltration of Thoulet's solution).

KCl solutions. Five concentrations (1, 5, 10, 100, and 1,000 mM) of KCl solutions were prepared for mass transport enhancement study using the current monitoring method (Pittman et al. 2002; Sze et al. 2003). Samples (n = 3) were incubated with deionized water for 24 h prior to the experiments, assuming that this resulted in enamel nanopores saturated with deionized water. By tracking the time taken for complete displacement of prefilled liquid A by B (when the current stabilized; see Fig. 2e), with known enamel specimen length, the average electro-osmotic flow velocity and the speed of infiltration were determined (Sze et al. 2003). The slope of the current-time curve can be expressed as:

$$gradient_{I-t} = \frac{\Delta I}{\Delta t} = \frac{A_c\left(\frac{V_{app}}{L}\right)\Delta\lambda_b + \Delta\lambda_s V_{app}}{\Delta t} = U_{ave}E_x\left(\frac{A_c}{L}\Delta\lambda_b + \Delta\lambda_s\right), \quad (1)$$

where U_{ave}, ΔI, and Δt are the average flow velocity and changes in current and time over the linear range; V_{app} is the applied voltage; λ is the conductivity; A is the cross-sectional area of the conducting media; and subscripts s and b are media

surface and bulk solution, respectively (see Appendix for detailed derivation of Eq. 1).

In the experiments to check for ion concentration polarization (ICP) phenomena (see Appendix), 1 test solution with fluorescent tracer was prepared by adding 1.55 mg/L of stock solution of Alexa Fluor 488 NHS Ester (Life Technologies, Thermo Fisher Scientific Inc., Waltham, MA, USA) to 5mM KCl test solution in 1:1,000 ratio. The EK infiltration test setup was used for both current-voltage (I-V) characteristic curve (n = 2) and fluorescent intensity (n = 1) measurements. Additionally, for fluorescence intensity measurement, the sample was mounted on an inverted microscope (Olympus IX71) equipped with a Hamamatsu Model Orca-AG CCD camera (Hamamatsu Photonics, Hamamatsu City, Japan). IPLab (Scanalytics, Rockville, MD, USA) was used for fluorescence intensity image acquisition, and captured images were analyzed using ImageJ software. More details are found in the Appendix.

Thoulet's solutions. Samples (n = 5) were incubated with 1mM KCl solution for 2 h to fill the enamel nanopores with relatively low–ionic strength solution (for higher EK flow speed and therefore faster infiltration). Then, the anodic reservoir solution was replaced by a high–ionic strength aqueous solution with mercuric and potassium iodide—Thoulet's solution (RI = 1.56, pH 6.5; 1.56 is the same RI of the organic matter in enamel). Infiltration of Thoulet's solution was carried out by mounting the enamel section on the chip and applying a voltage between anode (containing Thoulet's solution) and cathode reservoir (containing 1mM KCl solution). The infiltration process was monitored by birefringence measurement on the stage of a polarizing microscope (Olympus BX51), with or without a Red I interference filter, and the sample at the additional position of maximum birefringence (–45º to the north-south line). Optical retardance in nanometer (and observed birefringence) was measured with a Berek compensator before and after infiltration of Thoulet's solution at 30 histologic points (200 µm apart) to estimate the infiltrated volume. More details are found in the Appendix.

Resin infiltrant. A commercially available resin infiltrant (Icon, DMG, Hamburg, Germany) was infiltrated in enamel section samples (n = 8), with the same procedure described above. After the 2-h EK-driven infiltration period with resin infiltrant in the anode reservoir, the infiltrated samples were light cured (DX, Shanghai, China) for 2 min. A voltage of 5 V was used in the 2 infiltration periods. After infiltration, samples were submitted for (1) analysis by both fluorescence and polarizing microscopy to map the infiltrated area and quantify infiltration depth and (2) demineralization for 192 h via immersion in a solution of KH_2PO_4 (0.9 mmol/L), CH_3COOH (50 mmol/L), $CaCl_2$ (1.5 mmol/L), and sodium azide (0.02%) with pH 5.0 under constant stirring and at room temperature (22 ºC). The solution was changed every 24 h. At the infiltrated and noninfiltrated areas, mineral volume was measured by transverse microradiography (using the Angmar formula) at histologic points (n = 30 per area) before and after decalcification. See more details in the Appendix.

Whole Tooth Experiment with Resin Infiltrant

In 20 teeth, the enamel surface of the midcrown region was attached to a cylindrical reservoir (cured PDMS with 2 mm of diameter and 5 mm in length) containing the resin infiltrant in contact with the anode, and the cathode was inserted into the pulp chamber filled with a 70% glycerol gel (see below). A voltage of 2 V was applied for 2 h, and the PDMS device was removed and the infiltrated resin light cured for 2 min. Longitudinal ground sections were prepared both from the infiltrated area and from a noninfiltrated area at the opposing surface of each tooth, which were then analyzed by fluorescence microscopy to map the infiltrated area and to quantify the infiltration depth.

Statistical Analysis

The t test for paired samples (significance level of 5%) and the effect size for means were used to analyze (1) differences between observed birefringence before (in water) and after infiltration of Thoulet's solution and (2) mineral volume before and after in vitro demineralization of resin-infiltrated samples. Given that both in vitro demineralization (Anderson and Elliott 1987) and infiltration of Thoulet's solution (Houwink 1969) occur independently at histologic points within a same sample of dental enamel, sample sizes for statistical analysis were based on the number of histologic points and not on the number of ground sections.

Results

Microfluidic Chip Experiments with Enamel Ground Sections

KCl solutions. A typical current response (via current monitoring method) of 2-liquid displacement flow is shown in Figure 2e, where the current through the enamel slowly increases as the 1mM KCl initially present within the enamel nanopores is displaced by the incoming higher-conductivity 10mM KCl. With a field strength of ~800 V/m (i.e., 1 V across an approximately 1,260-µm sample length), the average flow velocity was 8.8×10^{-9} m/s (details are described in the Appendix).

Furthermore, characteristic features of ICP phenomenon were observed when a higher voltage was applied, in an attempt to accelerate the infiltration process (see Appendix Fig. 2). These features are (1) a formation of an ion depletion zone at the enamel-reservoir interface over time and (2) a typical I-V curve with 3 current regimes (ohmic, limiting, and overlimiting currents). Therefore, a supply voltage of 1 V was chosen for all KCl solutions used in enhanced mass transport experiments to minimize the formation of ICP effect.

Thoulet's solution. The initial-phase retardance of ~200 nm (birefringence of -20×10^{-4}) under water immersion changed (in all histologic points of all samples) to ~500 nm (birefringence of -50×10^{-4}) after infiltration of Thoulet's solution with

EK flow, following flow direction (Fig. 2f). Differences were statistically significant ($P < 0.00001$), with a large effect size (6.69; Appendix Fig. 3).

Resin infiltration. The infiltrated areas of enamel were more fluorescent and more birefringent than the noninfiltrated areas (Fig. 3a–c), with infiltration depths ranging from 700 to 1430 µm (median of 770 µm). After exposure to demineralization solution in vitro, mineral loss was much higher in noninfiltrated than in infiltrated sites ($P < 0.00001$; effect size of 3.26; Fig. 3d, f).

Whole Tooth Experiment with Resin Infiltrant

All samples presented positive current (typically 0.002 µA) during EK flow, indicating an active flow from the anode site to the cathode site. Ground sections of infiltrated area showed the enamel layer with a marked fluorescence area, whose morphology was compatible with the width of the reservoir on the tooth surface, while the enamel layer at the noninfiltrated areas was not fluorescent (Fig. 4b, c). The infiltration depth ranged from 1160 to 2190 µm (mean, 1630 µm ± 284 µm).

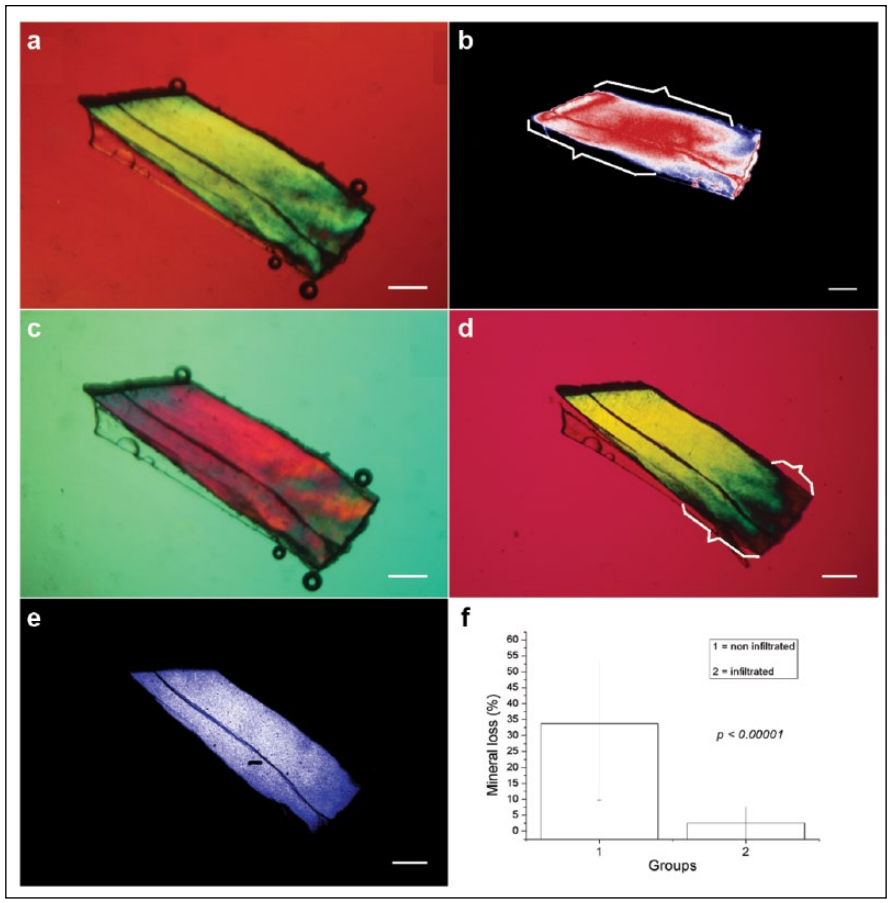

Figure 3. Representative findings of a ground section of normal dental enamel infiltrated with resin infiltrant by electrokinetic flow, from the left-hand side to the right. Soon after resin infiltration, the sample was immersed in water and then viewed under (**a**) polarized light microscopy (with 540-nm interference filter) and (**b**) fluorescence microscopy, showing two-thirds of the sample with a stronger fluorescence signal (see area marked by brackets). (**c**) The birefringence of the fluorescent area differentiates from that of the nonfluorescent area under polarized light microscopy (with a 680-nm retardance filter). In the same enamel section, (a) before and (**d**) after 192 h of decalcification, in vitro changes in interference color in the nonfluorescent area (see area marked with brackets) indicate that negative birefringence is reduced (less negative) and mineral loss was more significant in the noninfiltrated area. (**e**) Microradiography (in pseudocolors) confirms a lower radiopacity in the nonfluorescent area compared to the fluorescent one after 192 h of decalcification. Blue areas (less radiopaque) have lower mineral content. (**f**) Graph showing that mineral volume of resin-infiltrated histologic sites (test group; $n = 30$) did not change after exposure to decalcifying solution, while the noninfiltrated histologic sites (control group; $n = 30$) showed a statistically significant reduction ($P < 0.00001$) in mineral volume after decalcification with a high effect (effect size = 3.26). Histologic sites of analysis were distributed in 8 resin-infiltrated samples. Bars = 200 µm.

Discussion

A layer of excess of cations is found at the proximity of the negatively charged surface of nanochannels filled with aqueous solution, and the cations are mobilized toward the cathode side when an external electric field is applied. The content of the nanochannel is transported by the resulting flow, which is the basis for electro-osmotic flow. With low–ionic strength solutions, the electrical double layer is thick, resulting in overlapping at the center of the nanochannel, selectively excluding anions from the transport (Schoch et al. 2008). We first performed EK flow in enamel with low–ionic strength KCl solutions. An estimated EK flow velocity of 8.8×10^{-9} m/s was obtained. The corresponding infiltrated lengths after 3 h (10^4 s) of infiltration would be 100 µm (for EK-driven infiltration, with 8.8×10^{-9} m/s) and 1 µm (for diffusion-based infiltration with 2×10^{-10} cm^2/s). When enhanced infiltration was attempted by increasing applied voltage over time, limiting current behaviors that are characteristic of an ICP effect were observed, resulting mainly from exclusion of ions from the nanopores. One implication in dental research is that anions of remineralizing solutions with low ionic strengths are expected not to infiltrate into small enamel pores. This is consistent with (1) neutral molecules of remineralizing agents diffusing more preferably than charged ones through the highly mineralized surface layer of enamel caries (Cochrane et al. 2008) and (2) hindered diffusion caused by repulsion between charges of the solute and cylindrical pore walls (O-tane et al. 2011).

With Thoulet's solutions, which have high ionic strength (resulting in thin, possibly nonoverlapping electrical double layers), our tests resulted in the highest negative birefringence

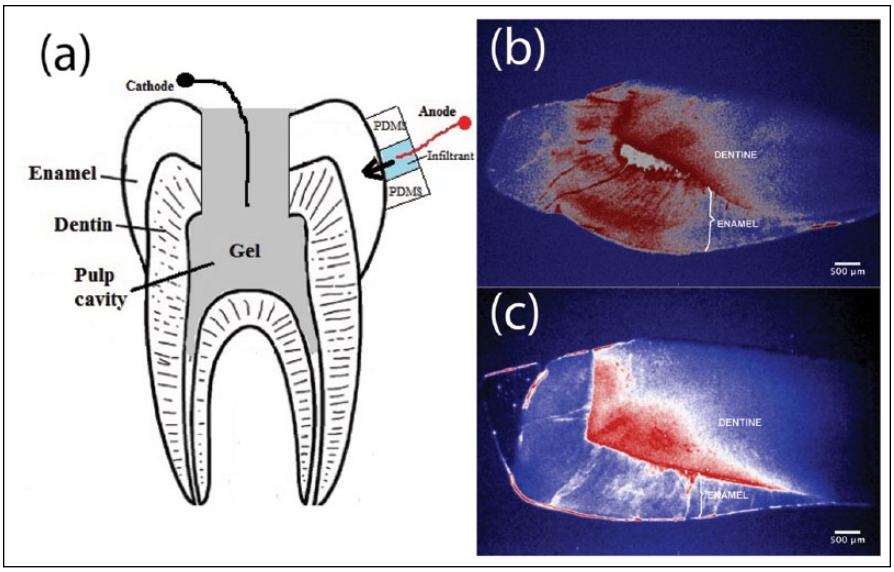

Figure 4. Whole tooth experiment. (**a**) Drawing describing the experimental setup of the whole tooth experiment. The dentin and enamel layers above the pulp chamber were mechanically removed with a dental bur, and the cavity that formed from the floor of the pulp chamber to the outer enamel layer was filled with a gel where a platinum wire (cathode) was inserted. On 1 tooth surface, at an opposite side to the pulp chamber, it was adhered a polydimethylsiloxane (PDMS) device with a central reservoir (2 mm in diameter) containing the infiltrant material (potassium chloride solution or resin) and another platinum wire (anode) so that the flow direction was from the tooth surface to the pulp chamber (arrow). (**b**, **c**) Typical fluorescence microscopy images (in pseudocolors) of tooth crown's ground sections of infiltrated (b) and noninfiltrated (c) surfaces from a same tooth of the whole tooth experiment (flow direction: from enamel surface inward; $n = 20$) with electrokinetic flow showing a resin-infiltrated enamel area (b; red) with the same depth of the enamel layer (1,800 µm; from enamel surface, at the lower outline of enamel, to the junction with dentine) in the center of the image. In actual in vivo implementation, the cathode (e.g., microneedle) can be inserted directly into the gum tissue without the removal of dental tissues.

(-50×10^{-4}) ever reported for normal enamel, suggesting significant infiltration of Thoulet's solution. The birefringence values for complete infiltration of Thoulet's solution with an RI of 1.56 in normal enamel (with mineral volume ranging from 88% to 98%) ranged from -45 to -55×10^{-4} as predicted from theory (Sousa et al. 2009). Previous studies on infiltration by diffusion of Thoulet's solution with high RIs (range, 1.53–1.62) reported either a negative birefringence lower than that in water, compatible with no infiltration (Angmar et al. 1963; Theuns et al. 1993), or a slight increase (up to 10%) in negative birefringence in normal enamel (Gwinnett 1966; Houwink 1969), even after 2 mo of immersion (Houwink 1969). The relatively high viscosities (which are inversely proportional to the diffusion rate; Dusenbury 2009) of Thoulet's solutions with high RI are probably responsible for a very low diffusion rate. Similar findings led researchers to conclude that the pores of normal enamel had radii smaller than those of dissolved ions (~0.5 nm; Theuns et al. 1993). Others have reported that the concentrated salt solutions not only failed to infiltrate but also caused an osmotic dehydration of normal enamel (Poole et al. 1981). Our results provide evidence that previous pore size estimates in enamel from diffusion experiments are misleading. On this basis, we tested the hypothesis that curable fluid resin could be infiltrated into normal enamel pores without pretreatment with acid.

Resin infiltration with EK flow resulted in penetration depths that are 1 to 2 orders of magnitude higher than that obtained by capillarity in acid-etched normal enamel (~10 µm; Van Meerbeek et al. 2003; Hannig et al. 2002), whose pores are enlarged compared to nonetched samples (Hannig et al. 2002). Infiltrated areas presented higher birefringence than noninfiltrated ones, indicating that infiltration occurred in the pore volume, not at the surfaces of the ground sections. The resistance to demineralization of infiltrated areas confirmed this as well. If infiltration had occurred only at the surfaces of the sample, acid would have diffused into enamel pores through the cathodic end and caused demineralization in the infiltrated areas.

Our experiments with the whole tooth resulted in a deeply infiltrated layer during a period compatible with a clinical dental appointment. As the cathode can be placed gently touching the oral mucosa surface (e.g., lips) and the procedure is painless (due to the very low current), there are potential applications in dentistry.

In contrast, the current infiltration requires acid pretreatment for enlarging enamel pores, which allow resin penetration by capillarity (Washburn 1921; Van Meerbeek et al. 2003). From the theory, the viscosity of the liquid and the capillary diameter are inversely and directly proportional to the penetration rate, respectively (Washburn 1921). The combination of the relatively high viscosity of the resin with the small diameter of normal enamel pores probably results in extremely low penetration rates of fluid resins into nonetched normal enamel, with limited applicability.

Conclusions

Our results with EK flow provide evidence of an improved transport of materials into normal dental enamel, including transportation of MACTs with no change in pore size, and a reduced infiltration of anions from solutions with low ionic strengths. This result has a direct impact on traditional thinking about the transport of materials in dental enamel, where transport improvement is attempted by other means, such as reducing molecular size, increasing pore size, and applying heat. Thus, properties of infiltrants can be altered to improve tooth color and the resistance of enamel to the oral environment, opening new avenues to improve oral health.

Author Contributions

H.Y. Gan, contributed to conception, design, data acquisition, analysis, and interpretation, drafted and critically revised the manuscript; F.B. Sousa, contributed to conception, data acquisition,

analysis, and interpretation, drafted and critically revised the manuscript; H.L. Carlo, P.P. Maciel, M.S. Marcena, contributed to data acquisition, drafted the manuscript; J. Han, contributed to conception and data interpretation, critically revised the manuscript. All authors gave final approval and agree to be accountable for all aspects of the work.

Acknowledgments

This work was supported by the Singapore-MIT Alliance II Flagship Research Project (Computational Engineering Program), as well as the MIT-Brazil-CNPq Seed Fund 2011 (551960/2011-6) and CNPq Universal Grant (480455/2012-0). H.Y. Gan was supported by a postdoctoral fellowship (2010–2012) from the Agency for Science, Technology and Research, Singapore. M.S. Macena was supported by the Sandwich Doctoral Scholarship of the MIT- Brazil-CNPq Seed Fund 2011 (551960/2011-6). P.P. Maciel was supported by a master scholarship from CAPES/ Brazilian Ministry of Education. We thank Rubenia Cristina de Medeiros for her help in preparing some ground sections of enamel. H.G., F.S., and J.H. applied for a patent based on the methodology described in the manuscript. The authors declare no potential conflicts of interest with respect to the authorship and/or publication of this article.

References

Anderson P, Elliott JC. 1987. Coupled diffusion as basis for subsurface demineralization in dental caries. Caries Res. 21:522–525.

Angmar B, Carlstrom D, Glas JE. 1963. Studies on the ultrastructure of dental enamel: IV. The mineralization of normal human enamel. J Ultrastruct Res. 8:12–23.

Cochrane NJ, Saranathan S, Cai F, Cross KJ, Reynolds EC. 2008. Enamel subsurface lesion remineralization with casein phosphopeptide stabilised solutions of calcium, phosphate and fluoride. Caries Res. 42:88–97.

De Medeiros RC, De Lima TA, Gouveia CR, De Sousa FB. 2013. Water loss at normal enamel histological points during air drying at room temperature. J Microsc. 250:218–227.

Duan C, Majumdar A. 2010. Anomalous ion transport in 2-nm hydrophilic nanochannels. Nat Nanotechnol. 5:848–852.

Dusenbury DB. 2009. Living at micro scale. Cambridge (MA): Harvard University Press.

Gwinnett AJ. 1966. Normal enamel: I. Quantitative polarized light study. J Dent Res. 45:120–127.

Hannig M, Bock H, Bott B, Hoth-Hannig W. 2002. Inter-crystallite nanoretention of self-etching adhesives at enamel imaged by TEM. Eur J Oral Sci. 110:464–470.

Houwink B. 1969. The limited usefulness of Thoulet's solution in imbibition experiments in dental enamel. Br Dent J. 126:447–450.

Ivanoff CS, Hottel TL, Garcia-Godoy F. 2012. Dielectrophoresis: a model to transport drugs directly into teeth. Electrophoresis. 33:1311–1321.

Ivanoff CS, Hottel TL, Tantbirojn DV, Versluis A, Garcia-Godoy F. 2011. Dielectrophoretic transport of fluoride into enamel. Am J Dent. 24:341–345.

Lee CY, Choi W, Han J-H, Strano MS. 2010. Coherence resonance in a single-walled carbon nanotube ion channel. Science. 329(5997):1320–1324.

Nanci A. 2012. Ten Cate's oral histology: development, structure, and function. New York (NY): Elsevier Health Sciences.

Pittman JL, Henry CS, Gilman SD. 2002. Experimental studies of electroosmotic flow dynamics in microfabricated devices during current monitoring experiments. Anal Chem. 75:361–370.

Poole DF, Newman HN, Dibdin GH. 1981. Structure and porosity of human cervical enamel studied by polarizing microscopy and transmission electron microscopy. Arch Oral Biol. 26:977–982.

Poole DF, Tailby PW, Berry DC. 1963. The movement of water and other molecules through human enamel. Arch Oral Biol. 8:771–772.

Schoch RB, Han J, Renaud P. 2008. Transport phenomena in nanofluidics. Rev Mod Phys. 80:839–883.

Shellis RP, Dibdin GH. 2000. Enamel microporosity and its functional implications. In: Teaford MF, Smith MM, Fergunson MW, editors. Development, function and evolution of teeth. New York (NY): Cambridge University Press. p. 242–251.

Sousa FB, Vianna SS, Santos-Magalhães NS. 2009. Dental enamel birefringence for a wide mineral content range and for different immersion media's refractive indexes: an improved mathematical interpretation. J Microsc. 233:69–75.

Sparreboom W, Berg Avd, Eijkel JC. 2012. Transport in nanofluidic systems: a review of theory and applications. New J Phys. 12. Article 015004.

Sze A, Erickson D, Ren L, Li D. 2003. Zeta-potential measurement using the Smoluchowski equation and the slope of the current-time relationship in electroosmotic flow. J Colloid Interface Sci. 261:402–410.

Theuns HM, Shellis RP, Groeneveld A, van Dijk JW, Poole DF. 1993. Relationships between birefringence and mineral content in artificial caries lesions of enamel. Caries Res. 27:9–14.

Van Meerbeek B, De Munck J, Yoshida Y, Inoue S, Vargas M, Vijay P, Van Landuyt K, Lambrechts P, Vanherle G. 2003. Adhesion to enamel and dentin: current status and future challenges. Oper Dent. 28:215–253.

Washburn EW. 1921. The dynamics of capillary flow. Phys Rev. 17:273–283.

Wu J, Gerstandt K, Zhang H, Liu J, Hinds BJ. 2012. Electrophoretically induced aqueous flow through single-walled carbon nanotube membranes. Nat Nanotechnol. 7:133–139.

Zahradnik RT, Moreno EC. 1975. Structural features of human enamel as revealed by isothermal water vapour sorption. Arch Oral Biol. 20:317–325.